# **Green Chemistry**



View Article Online **PAPER** 



Cite this: Green Chem 2018 20

Received 25th March 2018, Accepted 1st August 2018 DOI: 10.1039/c8gc00954f

rsc.li/greenchem

## Renewable energy storage via efficient reversible hydrogenation of piperidine captured CO<sub>2</sub>†

Mi Lu, 📵 Jianghao Zhang, Yao Yao, Junming Sun, Yong Wang and Hongfei Lin 📵 \*

The storage of renewable energy is the major hurdle during the transition of fossil resources to renewables. A possible solution is to convert renewable electricity to chemical energy carriers such as hydrogen for storage. Herein, a highly efficient formate-piperidine-adduct (FPA) based hydrogen storage system was developed. This system has shown rapid reaction kinetics of both hydrogenation of piperidinecaptured CO2 and dehydrogenation of the FPA over a carbon-supported palladium nano-catalyst under mild operating conditions. Moreover, the FPA solution based hydrogen storage system is advantageous owing to the generation of high-purity hydrogen, which is free of carbon monoxide and ammonia. In situ ATR-FTIR characterization was performed in order to provide insight into the reaction mechanisms involved. By integrating this breakthrough hydrogen storage system with renewable hydrogen and polymer electrolyte membrane fuel cells (PEMFC), in-demand cost-effective rechargeable hydrogen batteries could be realized for renewable energy storage.

The worldwide installed solar photovoltaic (PV) and wind energy system capacities have surged exponentially for the past few decades.1 However, wind and solar power generation is highly intermittent and seasonal, resulting in serious issues including grid capacity/stability, curtailment, and supply/ demand mismatch. One possible solution to the renewable electricity storage challenge is to use a regenerative hydrogen fuel cell (RHFC), which converts electricity to H2, a clean energy carrier that can be obtained from electrochemical water splitting,<sup>2</sup> and stores the H<sub>2</sub>, which is later fed into a fuel cell to regenerate electric power.3 Currently, hydrogen gas is commonly compressed and stored at an extremely high pressure (700 bar), leading to a high cost as well as safety concerns and logistical challenges since it is highly inflammable.<sup>4</sup> Chemical hydrogen storage options, including solid-state metal hydrides or liquid organic hydrogen carriers (LOHCs), could be a safe alternative to hydrogen storage.4c,5 However, the hydrogen release from these materials is strongly endothermic, typically requiring elevated temperatures of 150-500 °C, which are well above the "waste heat" temperature range of 80-90 °C provided by a standard PEMFC.

Formic acid (HCOOH) and formates have been considered as a promising material for chemical hydrogen storage because of their high volumetric capacities, which surpass

The Gene and Linda Voiland School of Chemical Engineering and Bioengineering, Washington State University, Pullman, WA 99164, USA.

E-mail: Honofei Lin@wsu edu

†Electronic supplementary information (ESI) available. See DOI: 10.1039/ c8gc00954f

those of most other chemical hydrogen storage materials.<sup>6</sup> Recently, immense progress has been made in the development of formate-based reversible H2 storage under mild conditions. 2b,7 Beller and co-workers suggested that the catalytic decomposition of a formate/amine adduct solution in the presence of homogeneous Ru catalysts as a practical H2 storage system for direct use in fuel cells.8 Hull et al. designed a reversible H<sub>2</sub> storage system with a homogeneous Ir catalyst, using pH to control H<sub>2</sub> production or consumption. Several reports also described the feasibility of using a homogeneous Ru catalyst to enable reversible HCOONa/NaHCO3-based H2 storage to achieve a higher volumetric density.10 Laurenczy's group designed a hydrogen battery system based on cesium formate/ bicarbonate due to the high solubility of cesium salts.7c However, due to the high cost arising from the use of sophisticated ligands and the limited recyclability, the homogeneous catalyst systems have not yet been ready for commercial applications.

Compared to the significant advances of homogeneously catalyzed, formate-based hydrogen storage systems, only few reports of using heterogeneous catalysts for hydrogen storage are available in the literature. Cao and co-workers<sup>11</sup> employed aqueous sodium formates as the H2 storage material over palladium on reduced graphitic oxide nanosheets (Pd/r-GO). 1c Notably, the rate of hydrogen discharge is too low for practical applications. 12 Recently, our group demonstrated a hydrogen storage system based on ammonium bicarbonate/formate redox equilibrium<sup>7d</sup> in aqueous media over the heterogeneous Pd/AC catalyst. This hydrogen storage system has an exceptionally high volumetric energy density (up to 168 g H<sub>2</sub> per L).

However, the challenge that trace amounts of CO and NH<sub>3</sub> could be formed by the decomposition of ammonium formate at elevated temperatures cannot be completely ruled out. 4c,7f,13 To further increase the power density, we found that adding alcohol as a co-solvent greatly enhances the kinetics of the hydrogenation of ammonium carbonate.<sup>14</sup> Herein, we have developed a new hydrogen storage system based on the formate piperidine adduct (FPA) solutions, in which the fast hydrogenation of captured CO<sub>2</sub> with piperidine to the FPA, as well as the rapid decomposition of the FPA for releasing highpurity H<sub>2</sub>, could be realized under mild conditions.

Table 1 shows the results of the catalytic hydrogenation of piperidine captured CO<sub>2</sub> in various aqueous ethanol solutions. After reacting for 1 hour in water at 20 °C (Table 1, entry 1), the yield of formate was 50.2%, and the corresponding turnover frequency (TOF) was approximately 1431 h<sup>-1</sup> over the activated carbon supported palladium catalyst (5 wt%, Pd/AC). Adding alcohol into a water solvent significantly improved the hydrogenation of piperidine captured CO<sub>2</sub>. For instance, the ethanol-water solution with 70 wt% ethanol exhibited a significant solvent promotion effect as a high yield of formate of ~83.6% was achieved in an hour at 20 °C, and the TOF reached up to ~3523 h<sup>-1</sup> over the Pd/AC catalyst (Table 1, entry 3). Moreover, a much higher yield of ~95.5% of formate was achieved by simply elevating the temperature from 20 °C to 30 °C (Table 1, entry 5). We found that other alcohols also have a similar promotion effect to ethanol. At 30 °C, by switching the aqueous ethanol solvent to the aqueous 1-propanol or the aqueous 2-propanol solvent, each containing 70 wt% alcohol, the formate yields reached ~96.4% and ~98.5%, respectively, in an hour (Table 1, entries 7 and 8).

In our previous studies, we considered that the promotion effect of the ethanol co-solvent can be attributed to: (1) the higher solubility of H<sub>2</sub> in ethanol than that in water;<sup>15</sup> and (2) the amount of bicarbonate and ethyl carbonate intermediate species which can be hydrogenated. Indeed, we observed an increasing trend of the formate yield as the ethanol content in

the aqueous solutions increased from 0% to 70%, but the yield then decreased as the ethanol content further increased to 100%. 13C NMR characterization (ESI, Fig. S1†) found that there was only one peak located at 161.2 ppm, which was assigned to the bicarbonate/carbonate ions after capturing CO<sub>2</sub> with piperidine in pure water. <sup>16</sup> In the ethanol-water mixed solvent, another peak located at 159.5 ppm appeared, which was assigned to ethyl carbonate ions. In pure ethanol, only the ethyl carbonate peak appeared. This observation is well consistent with our previous report that ethyl carbonate ions appear in the NH4HCO3 aqueous solutions when adding ethanol.14 However, the vield of formate decreased from ~83.6% in the aqueous ethanol solvent (an ethanol fraction of 70 wt%) to ~62.2% in pure ethanol, implying that an appropriate amount of water may enhance the hydrogenation performance. Interestingly, similar promotion effects by adding small amounts of water were observed in the CO2 hydrogenation reactions with homogeneous catalysts.<sup>17</sup> In general, under identical conditions, the maximum formate yield was obtained with the aqueous ethanol solvent at an optimal ethanol to water ratio, rather than with pure ethanol. However, the different properties of the solvents at various ethanol to water ratios likely influence the solubility of hydrogen, as well as the distribution of the bicarbonate and ethyl carbonate ions in the ethanol-water solvents, and therefore determine the optimal vield of formate.

Note that piperidine-carbamate was not observed from ex situ <sup>13</sup>C NMR characterization, although carbamate is readily formed by reacting CO2 with piperidine, a highly basic amine<sup>18</sup> (p $K_a$  = 11.28). Given the extended time (capturing CO<sub>2</sub> with piperidine lasted for 40 min in this study), piperidinecarbamate could be fully converted to bicarbonate<sup>19</sup> or ethyl carbonate in water or ethanol, respectively (Scheme 1). We also found that the CO2 hydrogenation rates were faster with piperidine than those with AMP under identical reaction conditions. Due to its strong basicity, piperidine acts as an electron-donating ligand which reduces the bonding energy of the

Table 1 Hydrogenation of piperidine-captured CO2 in different aqueous alcohol solutions

	Capture <sup>a</sup> and hydrogenation <sup>b</sup> Solvent (wt% alcohol)	Temperature (°C)	Captured $CO_2$ species concentration <sup>c</sup> (M)				Conversion results	
Entry			HCO <sub>3</sub>	CO <sub>3</sub> <sup>2-</sup>	RNCO <sup>2-</sup>	Alkyl-CO <sub>3</sub>	Formate yield (%)	$TOF^{d}(h^{-1})$
1	0% alcohol	20	0.93	0.03	0.00	0	50.2	1431
2	50% EtOH	20	0.73	0.01	0.01	0.21	78.0	3303
3	70% EtOH	20	0.32	0.00	0.03	0.61	83.6	3523
4	70% EtOH	25	0.32	0.00	0.03	0.61	87.4	4404
5	70% EtOH	30	0.32	0.00	0.03	0.61	95.5	5945
6	70% EtOH	40	0.32	0.00	0.03	0.61	70.5	3083
7	70% 1-propanol	30	0.30	0.00	0.03	0.62	96.4	4404
8	70% 2-propanol	30	0.30	0.00	0.03	0.62	98.5	5504
9	90% EtOH	20	0.03	0.00	0.03	0.90	80.4	3083
10	95.6% EtOH	20	0.01	0.00	0.03	0.92	68.6	2642
11	100% EtOH	20	0.00	0.00	0.03	0.93	62.2	2202

<sup>&</sup>lt;sup>a</sup> CO<sub>2</sub> capture conditions: 20 mL amine/water-ethanol, 1 M piperidine, 20 °C, 40 min. <sup>b</sup> Hydrogenation conditions: 50 mL Parr reactor, captured CO<sub>2</sub> solution (20 mL), 0.1 g Pd/AC (5 wt%), 400 psi hydrogen, 1 hour, 20 °C except entries 4–6. <sup>c</sup>The captured CO<sub>2</sub> species concentrations were determined by <sup>13</sup>C NMR spectroscopy. <sup>d</sup> The TOFs were calculated using: moles of formate/(moles of Pd × 23.2%)/reaction time. The dispersion of the Pd atoms on the surface of Pd NPs is 23.2%, which is determined by carbon monoxide chemisorption.

Paper Green Chemistry

Scheme 1 Proposed mechanism of the formation of piperidine–carbamate by capturing  $CO_2$  with piperidine and the subsequent conversion of piperidine–carbamate to the corresponding bicarbonate and ethyl carbonate salts in water and ethanol solvents, respectively.

formates on the Pd surface, and thus could improve the hydrogenation activity by enhancing the formate desorption, if the formate desorption would be the rate-limiting step. At the same time, electron donating piperidine also decreases the electron deficient character of the Pd nanocatalysts. <sup>20</sup> Therefore, it is also possible that piperidine altered the electronic states of Pd and thus promoted the hydrogenation reactions.

The temperature effect of the hydrogenation of piperidinecaptured CO<sub>2</sub> is shown in Table 1 (entries 3-6). The formate yield increased with increasing reaction temperature from 20 °C to 30 °C but then decreased with further increase in the reaction temperature to 40 °C. Generally speaking, higher reaction temperatures lead to faster hydrogenation kinetics. However, from the thermodynamics point of view, elevated temperatures favor the dehydrogenation reaction and thus shift the equilibrium to hydrogen evolution, which is in agreement with our previous study and the reports in the literature.<sup>21</sup> A detailed kinetic study on the hydrogenation of bicarbonate in pure water and ethyl carbonate in pure ethanol, respectively, has been performed. Both bicarbonate and ethyl carbonate were derived from piperidine-captured CO2. As shown in Fig. 1, in the temperature range of 20-40 °C, the activation energy ( $E_a$ ) is 64.1  $\pm$  2.1 kJ mol<sup>-1</sup> for the conversion of bicarbonate to formate in water, while it is slightly lower,  $56.2 \pm 3.2 \text{ kJ mol}^{-1}$ , for the hydrogenation of ethyl carbonate in absolute ethanol. Unlike the comparable activation energies of both reactions, the observed rate of the hydrogenation of ethyl carbonate in ethanol was an order of magnitude higher than that of the hydrogenation of bicarbonate in water, which is likely due to the increased solubility of H<sub>2</sub> in ethanol.

Besides studying the hydrogenation reactions, we also investigated the dehydrogenation of the FPA to close the hydrogen storage/evolution cycle. We conducted the dehydrogenation of the FPA (1 M in the aqueous solution with 70 wt% ethanol) in a relatively high temperature range under a  $N_2$  atmosphere at a pressure of 1 atm. As shown in Fig. 2, as the reaction temperature increased to 80 °C, the yield of hydrogen reached ~82% after 40 minutes. At 100 °C, a 92.1% yield of hydrogen was achieved after 40 min with a corresponding TOF of 9908 h<sup>-1</sup> within the initial 5 min. The activation energy of

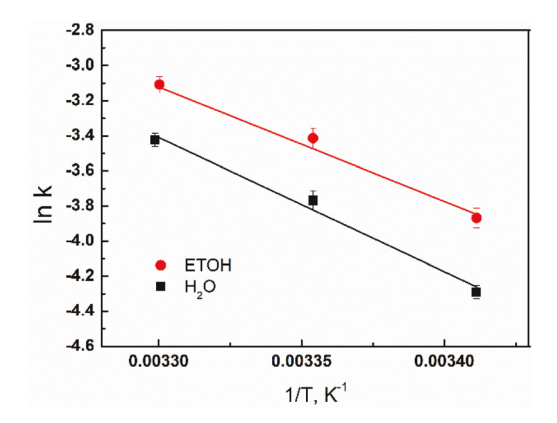


Fig. 1 Arrhenius plot of the hydrogenation of bicarbonate and ethyl carbonate in the presence of piperidine with 5 wt% Pd/AC in pure water and ethanol solvents, respectively. The reaction rates at different temperatures are shown in Fig. S2,† ESI. Reaction conditions: 1 M piperidine-captured  $CO_2$  in water or ethanol solution, 400 psi  $H_2$ , 1.0 g of Pd/AC.

the dehydrogenation was calculated to be 15 kJ mol<sup>-1</sup> (ESI, Fig. S3†). By switching the aqueous ethanol solvent (70 wt% ethanol) to either pure water or absolute ethanol, however, the generation rate of H2 gas from the FPA became slower (ESI, Fig. S4†). Similar to that in the hydrogenation reaction, ethanol also exhibits the co-solvent promotion effect in the dehydrogenation reaction due to the improvement of the solubility of reactants and intermediates, i.e., formates and ethyl carbonate. Whereas by using the aqueous propanol solvent containing 70 wt% alcohol, the hydrogen yield reached ~100% at 100 °C within only 30 min (ESI, Fig. S5†) with a record fast rate (TOF =  $1.21 \times 10^4 \text{ h}^{-1}$  within the initial 5 min) for discharging this hydrogen battery system, which results in an equivalent power density of 77.8 W kg<sup>-1</sup>. Besides hydrogen, nitrogen, and a minimal amount of CO2, no other gas was detected (CO detection limit is <1 ppm) (ESI, Fig. S6†). Thus, it was demonstrated that the same Pd/AC catalyst was active for

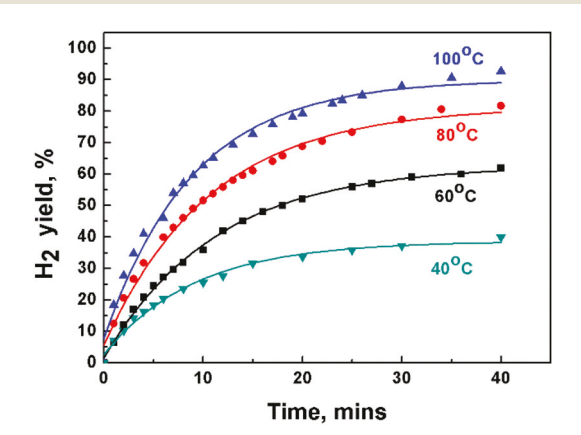


Fig. 2 Effect of different temperatures on the  $H_2$  releasing rate from the dehydrogenation of formate piperidine adducts. Reaction conditions: 0.1 g Pd/AC catalyst, 1 atm initial pressure of  $N_2$ , 1 M formate piperidine adducts, 20 mL aqueous solvent with 70% EtOH.

reversible  ${\rm CO_2}$  hydrogenation/formate dehydrogenation by varying the pressure and the reaction temperature.

It is generally accepted that adding base additives promotes both CO2 hydrogenation and formic acid dehydrogenation reactions. 2a,7e,22 Herein, the effect of the loading amount of piperidine on the formate dehydrogenation rate was investigated by varying the concentration of piperidine from 0 M to 5 M. A drastic increase of the hydrogen yield was observed as the concentration of piperidine increased from 0 M to 1 M, but the yield of H2 did not increase further with the increase in the piperidine concentration from 1 M to 5 M (ESI, Fig. S7†). This observation indicates a typical marginal effect of piperidine: once the formate piperidine adducts were formed, the excessive piperidine did not enhance the dehydrogenation rate. We also investigated the effect of different base types with varied basicity strengths on formate dehydrogenation. As shown in Fig. 3, the dehydrogenation rates with various bases were in the order of piperidine (p $K_a$  = 11.28)  $\approx$ NaOH (p $K_a = 13.8$ ) > AMP (p $K_a = 9.7$ )  $\approx$  MEA (p $K_a = 9.5$ ). It seems that given the same molar ratio of formic acid to the base, the higher the  $pK_a$  of the base, the faster was the dehydrogenation rate. From the thermodynamics point of view, the high  $pK_a$  of the base would decrease the free energy for both hydrogenation and dehydrogenation reactions.<sup>23</sup>

The decomposition of formates may involve multiple steps. Here, we used the kinetic isotope effect (KIE) measurements with HCOOH and DCOOH to determine the rate-limiting step and to understand the indispensable role of piperidine in facilitating the dehydrogenation (Table 2). We hypothesize that transient formate species adsorb on the Pd surface followed by critical formate dissociation (ESI, Scheme S1 $\dagger$ ). A general scheme of the dehydrogenation of formic acid involves decarboxylation, and thus  $CO_2$  and  $H_2$  are the final products. Adding an amine-like piperidine would facilitate the conversion of formate amine adducts to bicarbonates or ethyl carbonates. The deuterium kinetic isotopic effect (KIE) was higher with DCOOH-piperidine- $D_2O$  (KIE = 2.1, Table 2, entry 4) than

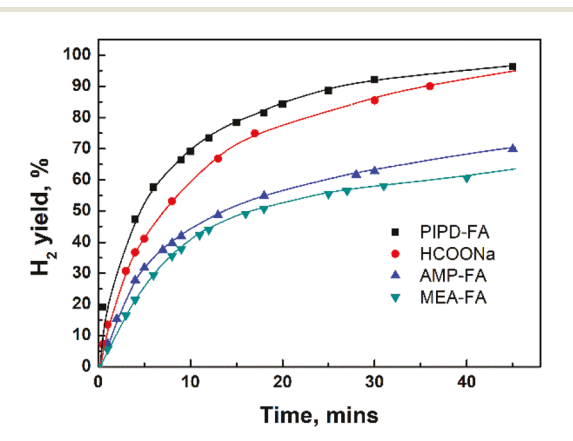


Fig. 3 Effect of different bases on the  $\rm H_2$  releasing rate from the dehydrogenation of formate piperidine adducts. Reaction conditions: 1 M formic acid mixed with 1 M of varied bases, 20 mL aqueous solutions with 70% EtOH, 0.1 g Pd/AC catalyst, 1 atm initial pressure of  $\rm N_2$ , 100 °C.

**Table 2** Deuterium kinetic isotopic effect study. Reaction conditions: 10 mL 0.5 M PIPD-DCOOH or HCOOH solutions in  $H_2O$  or  $D_2O$ , 0.1 g Pd/AC catalyst, 0.1 MPa initial  $N_2$  pressure, 40 °C, 0–40 min. Reactions were repeated three times

Entry	Substrate/solvent	Reaction rate (M s <sup>-1</sup> )	KIE
1	HCOOH-piperidine/H <sub>2</sub> O	0.002076	1.0
2	HCOOH-piperidine/D <sub>2</sub> O	0.001946	1.1
3	DCOOH-piperidine/H <sub>2</sub> O	0.001297	1.6
4	DCOOH-piperidine/D <sub>2</sub> O	0.000973	2.1

that with HCOOH-piperidine–D<sub>2</sub>O (KIE = 1.1, Table 2, entry 2), showing that the cleavage of the C–H bond in formate is the rate-limiting step for the decomposition of the FPA. Note that the conjugated acid of piperidine, in association with the piperidine-H<sup>+</sup> (PIPDH<sup>+</sup>) species formed *via* the reaction of piperidine with formic acid, as a proton donor can also facilitate the protonation of the adsorbed formate species, leading to the formation of a Pd-bicarbonate/ethyl carbonate species during the dehydrogenation reaction. The Pd-bicarbonate/ethylcarbonate complex might undergo further desorption from the Pd surface and become the ionic species in the solvents.<sup>24</sup> At elevated temperatures, bicarbonate or ethyl carbonate ions are readily decomposed to produce CO<sub>2</sub>, which was detected in the dehydrogenation reactions at temperatures higher than 40 °C.

To gain insight into the nature of surface intermediates during the FPA dehydrogenation reactions, the Pd/AC catalyst samples were further characterized during the reaction by *in situ* ATR-FTIR. We first recorded the IR spectra of the Pd/AC catalyst when CO flowed through the ATR cell to confirm the position of CO absorbance. A small peak was observed at ~2020 cm<sup>-1</sup> (ESI, Fig. S8†), which can be assigned to linearly adsorbed CO.<sup>25</sup> We then recorded the spectra of the Pd/AC catalyst in the reactive environment for the dehydrogenation of the FPA. Notably, as shown in Fig. 4, no peak in the 1800–2100 cm<sup>-1</sup> range (region of chemisorbed CO)<sup>25</sup> was observed during the dehydrogenation of the FPA, which may

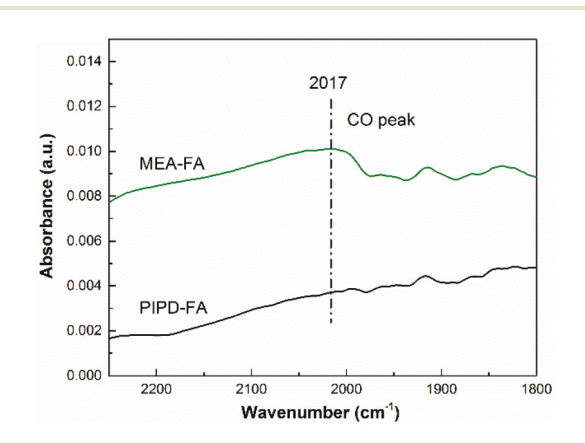


Fig. 4 ATR-FTIR spectra recorded during the dehydrogenation of formate with MEA and piperidine, respectively, at 55 °C.

be because piperidine suppressed the formation of CO. Boitiaux et al. also reported that piperidine exhibited a ligand effect and thus suppressed the CO formation during the hydrogenation reactions.20 This is a crucial feature because CO could occupy the active sites on the Pd catalyst surface as a poisoner and consequently deactivate the catalyst. Also, no CO formation during H2 evolution is indispensable in a PEM fuel cell since a trace amount of CO would poison the Pt cathode. In contrast, the CO peak was observed during the decomposition of monoethanolamine (MEA)-formate. The above observation suggests that piperidine could inhibit the undesired reaction to form CO, while largely promoting the rate of H<sub>2</sub> generation. Note that the  $pK_a$  of PIPDH<sup>+</sup> is 11.28, which is larger than that of MEAH<sup>+</sup> (p $K_a = 9.45$ ). Therefore the electrondonating ability of PIPD should be stronger than that of MEA. We speculate that the stronger electron-donating ability could facilitate the CO desorption from the catalyst surface. Both the spectra of PIPD and MEA showed a negative peak at 1589 cm<sup>-1</sup>, which is assigned to the vibrations of a surfacebound formate species, 26 indicating that the formate species on the catalyst surface was gradually consumed. Based on the intensity of this peak, the decomposition of the formate with PIPD was completed in 40 min since no further growth of this negative peak was detected after 40 min. As for the spectra of MEA, the intensity of the peak at 1589 cm<sup>-1</sup> reached a plateau after 1 h. However, this peak is much smaller than that of piperidine which suggests that the MEA formate adduct was not completely decomposed, and instead, the reaction stopped (ESI, Fig. S9 and S10†). We thus conclude that, due to the CO poisoning, the Pd/AC catalyst for the dehydrogenation of MEA-formate was deactivated with a prolonged reaction time, which is consistent with the low yield of hydrogen as shown in Fig. 3.

As shown in Fig. S8 and S9,† the negative peaks at 1375 and 1346 cm<sup>-1</sup> are ascribed to the C-O vibrations in HCO<sub>3</sub><sup>-</sup>, CH<sub>3</sub>CH<sub>2</sub>CO<sub>3</sub> and HCOO, respectively, whose intensity increases with the reaction time. However, in the whole spectra, no C-N stretching vibration band (usually at ~1645 and 1518 cm<sup>-1</sup>)<sup>27</sup> was observed since there was no consumption or re-formation of piperidine, which indeed acted as a cocatalyst during the reaction. Note that these carbonyl compounds were likely displayed as monodentates<sup>28</sup> on the surface of the Pd catalyst in our reaction system (Scheme S1†). In contrast, in a high-temperature gas-phase reaction, the bidentate forms of formate adsorbed on the Pd surface usually appear at higher wavenumbers. 25,26a

After 5 cycles of hydrogenation-dehydrogenation cycling tests, the loss of catalyst activities appeared to be negligible, as shown in Fig. 5. Moreover, piperidine did not decompose at 100 °C during the dehydrogenation reaction (ESI, Fig. S11†). The excellent stability of both the Pd/AC catalyst and the piperidine solvents suggests that the PFA-based, heterogeneously catalyzed hydrogen storage system is promising in terms of recyclability and reusability. Based on the current best H<sub>2</sub> production rates from this study (Table 1), producing 1 kW of electric power would require 5.4 L of the 1 M piperidine

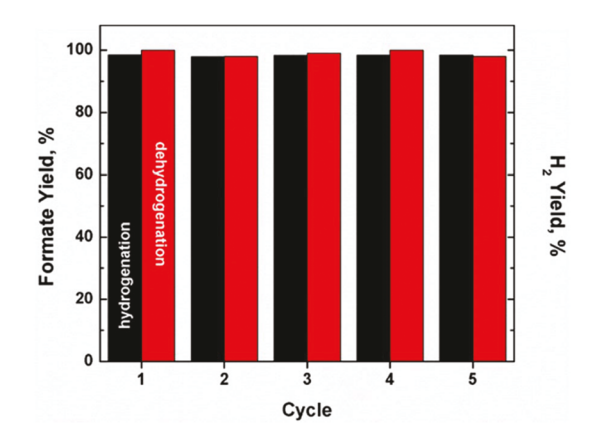


Fig. 5 Stability test of the Pd/AC catalyst for 5 cycles of hydrogenation-dehydrogenation. Hydrogenation of PIPD-CO<sub>2</sub>: 70% 2-propanol, 0.1 g Pd/AC, 30 °C, 1 hour; dehydrogenation of PIPD-formic acid: 70% 2-propanol, 0.1 g Pd/AC, 100 °C, 30 min. The spent Pd/AC catalyst was reused without regeneration.

formate solution or 0.69 L of the saturated piperidine formate solution (7.6 M at 25 °C), using approximately 27 g of 5 wt% Pd/AC.

#### Conclusions

In conclusion, we demonstrated that a highly efficient reversible hydrogen storage approach can be realized based on the piperidine formate adducts, which are produced by the hydrogenation of piperidine-captured CO2, in aqueous alcohol solutions. As for hydrogen charging, piperidine-captured CO<sub>2</sub> shows that the superior hydrogenation reactivity, ~95.5% formate yield, could be obtained in the ethanolwater solution (70 wt% alcohol) with 400 psi H2 after reacting for 1 hour at 30 °C. The kinetic rate of the reverse reaction, hydrogen discharging via dehydrogenation of the piperidine formate adduct in aqueous alcohol solutions, was also fast. The yield of high-purity  $H_2$  reached  ${\sim}100\%$  in 40 min at 100 °C. The impurities such as CO, NH<sub>3</sub> or piperidine were not detected in the discharged H<sub>2</sub>. The deuterium kinetic isotopic study found that the cleavage of the C-H bond in the formate is the rate-limiting step. The mechanistic study by in situ ATR-FTIR characterization discovered that piperidine improves both hydrogenation and dehydrogenation reactivity and no surface bound CO was formed during the dehydrogenation reactions. We also found that the Pd/ AC catalyst is highly stable and easy to handle and recycle, and so is piperidine. The storage of renewable energy can thus be realized through the "hydrogen battery", in which the piperidine formate adduct solutions store the hydrogen generated via water splitting with electrical energy from renewable resources such as solar, wind, geothermal energy etc.

Green Chemistry Paper

#### Conflicts of interest

There are no conflicts to declare.

### Acknowledgements

This material is based on work supported by the National Science Foundation under grant no. CBET 1748579. The authors thank Dr Steven Spain at the University of Nevada, Reno for the chemical analysis using the NMR facilities in the Shared Instrumentation Laboratory (SIL). The authors also thank Dr Zhenglong Li and Dr Michael Hu at Oak Ridge National Laboratory for useful discussions.

#### Notes and references

- (a) IEA, Technology Roadmap: Solar Photovoltaic Energy,
   2014; (b) GWEC, Global wind statistics 2014, 2015;
   (c) Q. Y. Bi, J. D. Lin, Y. M. Liu, X. L. Du, J. Q. Wang,
   H. Y. He and Y. Cao, Angew. Chem., Int. Ed., 2014, 53,
   13583-13587; (d) K. Christopher and R. Dimitrios, Energy Environ. Sci., 2012, 5, 6640.
- (a) S. Enthaler, J. von Langermann and T. Schmidt, Energy Environ. Sci., 2010, 3, 1207; (b) J. Kothandaraman, M. Czaun, A. Goeppert, R. Haiges, J.-P. Jones, R. B. May, G. K. S. Prakash and G. A. Olah, ChemSusChem, 2015, 8, 1442–1451.
- 3 (a) G. Cau, D. Cocco, M. Petrollese, S. Knudsen Kær and C. Milan, *Energy Convers. Manage.*, 2014, **87**, 820–831; (b) G. Gahleitner, *Int. J. Hydrogen Energy*, 2013, **38**, 2039–2061.
- 4 (a) L. Schlapbach and A. Züttel, *Nature*, 2001, 414, 353–358; (b) M. A. Rosen, *Hydrogen Production, Prospects and Processes*, 2012, vol. 1, pp. 10–29; (c) M. Yadav and Q. Xu, *Energy Environ. Sci.*, 2012, 5, 9698–9725.
- 5 (a) J. Yang, A. Sudik, C. Wolverton and D. J. Siegel, Chem. Soc. Rev., 2010, 39, 656-675; (b) C. W. Hamilton, R. T. Baker, A. Staubitz and I. Manners, Chem. Soc. Rev., 2009, 38, 279-293; (c) K. M. Eblagon, D. Rentsch, O. Friedrichs, A. Remhof, A. Zuettel, A. J. Ramirez-Cuesta and S. C. Tsang, Int. J. Hydrogen Energy, 2010, 35, 11609-11621; (d) W. Luo, P. G. Campbell, L. N. Zakharov and S.-Y. Liu, J. Am. Chem. Soc., 2011, 133, 19326-19329.
- 6 (a) M. Grasemann and G. Laurenczy, Energy Environ. Sci.,
  2012, 5, 8171; (b) P. Sponholz, D. Mellmann, H. Junge and
  M. Beller, ChemSusChem, 2013, 6, 1172–1176; (c) F. Joó,
  ChemSusChem, 2008, 1, 805–808.
- 7 (a) H. Horváth, G. Papp, R. Szabolcsi, Á. Kathő and F. Joő, ChemSusChem, 2015, 8, 3036–3038; (b) Q. Liu, X. Yang, Y. Huang, S. Xu, X. Su, X. Pan, J. Xu, A. Wang, C. Liang, X. Wang and T. Zhang, Energy Environ. Sci., 2015, 8, 3204–3207; (c) K. Sordakis, A. F. Dalebrook and G. Laurenczy, ChemCatChem, 2015, 7, 2332–2339; (d) J. Su, L. Yang, M. Lu and H. Lin, ChemSusChem, 2015, 8, 813–816; (e) G. A. Filonenko, R. Van Putten, E. N. Schulpen,

- E. J. M. Hensen and E. A. Pidko, ChemCatChem, 2014, 6, 1526-1530; (f) K. Jiang, K. Xu, S. Zou and W.-B. Cai, J. Am. Chem. Soc., 2014, 136, 4861-4864; (g) S. F. Hsu, S. Rommel, P. Eversfield, K. Muller, E. Klemm, W. R. Thiel and B. Plietker, Angew. Chem., Int. Ed., 2014, 53, 7074-7078; (h) P. Hu, E. Fogler, Y. Diskin-Posner, M. A. Iron and D. Milstein, Nat. Commun., 2015, 6, 6859; (i) P. Hu, Y. Ben-David and D. Milstein, Angew. Chem., Int. Ed., 2016, 55, 1061–1064; (j) A. L. Wang, O. Naoya, K. Murata, T. Hirose, J. T. Muckerman, E. Fujita, Y. Himeda, L. Wang, N. Onishi, K. Murata, T. Hirose and J. T. Muckerman, ChemSusChem, 2017, **10**, 1071–1075; (k) D. Forberg, T. Schwob, M. Zaheer, M. Friedrich, N. Miyajima and R. Kempe, Nat. Commun., 2016, 7, 13201; (l) K. Koh, M. Jeon, D. M. Chevrier, P. Zhang, C. W. Yoon and T. Asefa, Appl. Catal., B, 2017, 203, 820-828; (m) D. Mellmann, P. Sponholz, H. Junge, M. Beller, J. Skea, N. Armaroli, V. Balzani, N. Armaroli, V. Balzani, N. Armaroli, et al., Chem. Soc. Rev., 2016, 45, 3954-3988.
- 8 (a) A. Boddien, B. Loges, H. Junge, F. Gärtner, J. R. Noyes and M. Beller, *Adv. Synth. Catal.*, 2009, 351, 2517–2520;
  (b) B. Loges, A. Boddien, H. Junge and M. Beller, *Angew. Chem.*, 2008, 47, 3962–3965.
- 9 J. F. Hull, Y. Himeda, W.-H. Wang, B. Hashiguchi, R. Periana, D. J. Szalda, J. T. Muckerman and E. Fujita, *Nat. Chem.*, 2012, 4, 383–388.
- 10 G. Papp, J. Csorba, G. Laurenczy and F. Joó, *Angew. Chem.*, 2011, **50**, 10433–10435.
- 11 Q.-Y. Bi, J.-D. Lin, Y.-M. Liu, X.-L. Du, J.-Q. Wang, H.-Y. He and Y. Cao, *Angew. Chem.*, 2014, **53**, 13583–13587.
- 12 E. Hosono, T. Kudo, I. Honma, H. Matsuda and H. Zhou, *Nano Lett.*, 2009, **9**, 1045–1051.
- 13 J. Su, M. Lu and H. Lin, Green Chem., 2015, 17, 2769-2773.
- 14 W. H. Wang, S. Xu, Y. Manaka, Y. Suna, H. Kambayashi, J. T. Muckerman, E. Fujita and Y. Himeda, *ChemSusChem*, 2014, 7, 1976–1983.
- 15 R. M. Deshpande, R. V. Chaudhari and H. Delmas, *J. Chem. Eng. Data*, 1996, **41**, 1414–1417.
- 16 P. Holms, M. NAAZ and B. Poling, *Ind. Eng. Chem. Res.*, 1998, 37, 3281–3287.
- 17 (a) G. A. Filonenko, M. P. Conley, C. Copéret, M. Lutz, E. J. M. Hensen and E. A. Pidko, ACS Catal., 2013, 3, 2522–2526; (b) P. G. Jessop, Y. Hsiao, T. Ikariya and R. Noyori, J. Am. Chem. Soc., 1996, 118, 344–355; (c) Z. Xu, N. D. Mcnamara, G. T. Neumann, W. F. Schneider and J. C. Hicks, ChemCatChem, 2013, 5, 1769–1771.
- 18 P. V. Kortunov, L. S. Baugh, M. Siskin and D. C. Calabro, Energy Fuels, 2015, 29, 5967–5989.
- (a) K. Robinson, A. McCluskey and M. I. Attalla, *ChemPhysChem*, 2011, 12, 1088–1099; (b) P. V. Kortunov, M. Siskin, L. S. Baugh and D. C. Calabro, *Energy Fuels*, 2015, 29, 5919–5939.
- 20 J. Boitiaux, J. Cosyns and S. Vasudevan, *Appl. Catal.*, 1985, **15**, 317–326.
- 21 (a) H. Wiener, Y. Sasson and J. Blum, *J. Mol. Catal.*, 1986, 35, 277–284; (b) B. Zaidman, H. Wiener and Y. Sasson,

- *Int. J. Hydrogen Energy*, 1986, **11**, 341–347; (*c*) B. Zaidman, H. Wiener and Y. Sasson, *Sol. Energy*, 1989, 291–296.
- 22 Z. Zhang, S. Hu, J. Song, W. Li, G. Yang and B. Han, *ChemSusChem*, 2009, 2, 234–238.
- 23 D. B. Lao, B. R. Galan, J. C. Linehan and D. J. Heldebrant, *Green Chem.*, 2016, **18**, 4871–4874.
- 24 Q. Bi, X. Du, L. He, Y. Liu, Y. Cao, H. He and K. Fan, *J. Am. Chem. Soc.*, 2012, **134**, 8926–8933.
- 25 G. C. Cabilla, A. L. Bonivardi and M. A. Baltanais, *J. Catal.*, 2001, **201**, 213–220.
- 26 (a) V. Arunajatesan, B. Subramaniam, K. W. Hutchenson and F. E. Herkes, *Chem. Eng. Sci.*, 2007, 62, 5062–5069;
  (b) J. Araña, C. Garriga I Cabo, J. M. Doña-Rodríguez, O. González-Díaz, J. A. Herrera-Melián and J. Pérez-Peña, *Appl. Surf. Sci.*, 2004, 239, 60–71.
- 27 (a) K. Robinson, A. McCluskey and M. I. Attalla, ChemPhysChem, 2011, 12, 1088–1099; (b) G. Richner and G. Puxty, Ind. Eng. Chem. Res., 2012, 51, 14317–14324.
- 28 A. C. C. Chang, S. S. C. Chuang, M. Gray and Y. Soong, *Energy Fuels*, 2003, 17, 468–473.